

Matter waves from quantum sources in a force field

This article has been downloaded from IOPscience. Please scroll down to see the full text article.

2002 J. Phys. A: Math. Gen. 35 8361

(<http://iopscience.iop.org/0305-4470/35/40/301>)

View [the table of contents for this issue](#), or go to the [journal homepage](#) for more

Download details:

IP Address: 171.66.16.109

The article was downloaded on 02/06/2010 at 10:32

Please note that [terms and conditions apply](#).

Matter waves from quantum sources in a force field

T Kramer, C Bracher¹ and M Kleber

Physik-Department T30, Technische Universität München, James-Franck-Straße,
85747 Garching, Germany

E-mail: tkramer@ph.tum.de

Received 27 November 2001

Published 24 September 2002

Online at stacks.iop.org/JPhysA/35/8361

Abstract

Localized scattering phenomena may result in the formation of stationary matter waves originating from a compact region in physical space. Mathematically, such waves are advantageously expressed in terms of quantum sources that are introduced into the Schrödinger equation. The source formalism yields direct access to the scattering wavefunction, particle distribution and total current. As an example, we study emission from three-dimensional Gaussian sources into a homogeneous force field. This model describes the behaviour of an atom laser supplied by an ideal Bose–Einstein condensate under the influence of gravity. We predict a strong dependence of the beam profile on the condensate size and the presence of interference phenomena recently observed in photodetachment experiments.

PACS numbers: 03.75.–b, 03.65.Nk, 32.80.Gc

1. Introduction

Sources of particles are known to be an indispensable element in all scattering experiments. Located far away from the scattering region, sources will give rise to boundary conditions on the scattering wavefunction in the form of incoming plane waves. However, sources that are close to or within the relevant interaction region should be introduced directly into the Schrödinger equation [1]. More generally, the concept of a particle source arises naturally if a complex quantum process can be decomposed into several steps, where the preparation of the state under consideration is separated from its further evolution in an external field. For example, in intense-field laser–atom physics, the laser interacts with a pool of atoms in a complicated nonlinear way. As a result of this process a coherent source of above-threshold electrons is generated that will emit electrons in the form of an outgoing spherical wave with a given energy in the continuum [2–4].

¹ Present address: Department of Physics and Atmospheric Science, Dalhousie University, Halifax, N.S, Canada, B3H 3J5.

In this article we discuss in more detail a stationary quantum source that allows for a fully analytical solution. Our novel example predicts how the properties of the resulting matter waves are controlled by the size of the underlying source. The model we are presenting is surprisingly simple: a weak, harmonic perturbation couples the bound state in an isotropic oscillator potential to a continuum state experiencing a homogeneous force field. In section 2, we show how the ground-state wavefunction acts as a stationary quantum source for the uniformly accelerated scattering wave, and discuss the ensuing integrated current and current distribution. For a three-dimensional Gaussian source embedded in a linear potential environment, an exact solution for the emitted wave and the associated current is obtained in section 3, which allows for a pictorial interpretation in terms of a ‘virtual’ point source. In section 4, this theory serves as a simple model for two phenomena recently investigated experimentally, the formation of a freely falling ‘atom laser’ beam from a trapped Bose–Einstein condensate, and near-threshold photodetachment microscopy of negative ions in an electric field. Finally, a brief outlook is given in section 5.

2. Quantum sources in an external field

To motivate the quantum source approach, we shall introduce a two-state model with time-independent Hamiltonians. One state is a bound state of the Hamiltonian H_{trap} ; the second state is a scattering state of the Hamiltonian H_{cont} containing an external potential. The two states have an energy difference of $\Delta E = E_{\text{cont}} - E_{\text{trap}}$ and are weakly coupled by a homogeneous but oscillating interaction potential of strength $\hbar\Omega$:

$$(i\hbar\partial_t - H_{\text{cont}})\psi_{\text{cont}}(\mathbf{r}, t) = \hbar\Omega e^{-i\Delta Et/\hbar}\psi_{\text{trap}}(\mathbf{r}, t) \quad (1)$$

$$(i\hbar\partial_t - H_{\text{trap}})\psi_{\text{trap}}(\mathbf{r}, t) = \hbar\Omega e^{+i\Delta Et/\hbar}\psi_{\text{cont}}(\mathbf{r}, t). \quad (2)$$

We split off the time dependence of the states

$$\psi_{\text{cont}}(\mathbf{r}, t) = e^{-iE_{\text{cont}}t/\hbar}\psi_{\text{cont}}(\mathbf{r}) \quad (3)$$

$$\psi_{\text{trap}}(\mathbf{r}, t) = e^{-iE_{\text{trap}}t/\hbar}\psi_{\text{trap}}(\mathbf{r}), \quad (4)$$

to obtain the stationary equations

$$(E_{\text{cont}} - H_{\text{cont}})\psi_{\text{cont}}(\mathbf{r}) = \hbar\Omega\psi_{\text{trap}}(\mathbf{r}) \quad (5)$$

$$(E_{\text{trap}} - H_{\text{trap}})\psi_{\text{trap}}(\mathbf{r}) = \hbar\Omega\psi_{\text{cont}}(\mathbf{r}). \quad (6)$$

Upon introducing a suitable energy-dependent Green function $G_{\text{cont}}(\mathbf{r}, \mathbf{r}'; E)$ for H_{cont} (see section 2.2)

$$(E - H_{\text{cont}})G_{\text{cont}}(\mathbf{r}, \mathbf{r}'; E) = \delta(\mathbf{r} - \mathbf{r}'), \quad (7)$$

the formal solution of equation (5) is given by

$$\psi_{\text{cont}}(\mathbf{r}) = \hbar\Omega \int d^3r' G_{\text{cont}}(\mathbf{r}, \mathbf{r}'; E_{\text{cont}}) \psi_{\text{trap}}(\mathbf{r}'). \quad (8)$$

A similar equation holds for $\psi_{\text{trap}}(\mathbf{r})$. However, if we assume only a weak interaction in the sense that $\psi_{\text{trap}}(\mathbf{r})$ is not changed appreciably by the interaction, we may as a first approximation replace $\psi_{\text{trap}}(\mathbf{r})$ in equation (8) by the bound eigenstate $\psi_0(\mathbf{r})$ of H_{trap} , which is defined by

$$(E_0 - H_{\text{trap}})\psi_0(\mathbf{r}) = 0. \quad (9)$$

In this way we have decoupled the two equations and we obtain a new Schrödinger equation with an inhomogeneous source term $\sigma(\mathbf{r}) = \hbar\Omega\psi_0(\mathbf{r})$

$$(E_{\text{cont}} - H_{\text{cont}})\psi_{\text{cont}}(\mathbf{r}) = \sigma(\mathbf{r}). \quad (10)$$

From now on we shall suppress the label *cont*, since we are not interested in the propagation of the bound state. Therefore the rewritten equation (8)

$$\psi(\mathbf{r}) = \int d^3\mathbf{r}' G(\mathbf{r}, \mathbf{r}'; E) \sigma(\mathbf{r}') \quad (11)$$

serves as the starting point for our development of the theory of quantum sources.

2.1. Currents from sources

We associate a probability current density $\mathbf{j}(\mathbf{r})$ with the scattering wave $\psi(\mathbf{r})$ via

$$\mathbf{j}(\mathbf{r}) = \frac{\hbar}{m} \text{Im} \{ \psi(\mathbf{r})^* \nabla \psi(\mathbf{r}) \} - \frac{e\mathbf{A}(\mathbf{r})}{m} |\psi(\mathbf{r})|^2, \quad (12)$$

where $\mathbf{A}(\mathbf{r})$ denotes the vector potential. Together with equation (10) it is straightforward to derive the equation of continuity for this stationary problem:

$$\nabla \cdot \mathbf{j}(\mathbf{r}) = -\frac{2}{\hbar} \text{Im} \{ \sigma(\mathbf{r})^* \psi(\mathbf{r}) \}. \quad (13)$$

Note that the introduction of sources $\sigma(\mathbf{r})$ in the Schrödinger equation (10) causes the appearance of a source term in the equation of continuity that depends on the wavefunction $\psi(\mathbf{r})$. By integration over a surface enclosing the source we obtain a bilinear expression for the total probability current carried by $\psi(\mathbf{r})$:

$$J(E) = -\frac{2}{\hbar} \text{Im} \left\{ \int d^3\mathbf{r} \int d^3\mathbf{r}' \sigma(\mathbf{r})^* G(\mathbf{r}, \mathbf{r}'; E) \sigma(\mathbf{r}') \right\}. \quad (14)$$

This quantity details the total cross section of the underlying scattering process.

2.2. The energy-dependent Green function

For our stationary problem, the mathematical formulation of source theory heavily relies on the energy-dependent Green function $G(\mathbf{r}, \mathbf{r}'; E)$ of the Hamiltonian. In the continuous spectrum of H , however, this integral kernel is by no means unique. From a physical point of view, this ambiguity of the solution set (11) is required to accommodate different boundary conditions for the resulting wavefunction $\psi(\mathbf{r})$. Here, we are interested in outgoing matter waves that enforce the use of the retarded energy Green function [5]. (This choice of kernel guarantees the correct sign for the total current $J(E)$ (14), as shown by an eigenfunction expansion of $G(\mathbf{r}, \mathbf{r}'; E)$ [6].) For reasons of causality, the retarded energy Green function is connected to the propagator $K(\mathbf{r}, t|\mathbf{r}', 0)$ of the equivalent time-dependent problem by the Laplace transform:

$$G(\mathbf{r}, \mathbf{r}'; E) = \frac{1}{i\hbar} \int_0^\infty dt e^{iEt/\hbar} K(\mathbf{r}, t|\mathbf{r}', 0). \quad (15)$$

The time-dependent quantum propagator is a thoroughly studied subject, and a fairly exhaustive list of available solutions is given in [7, 8]. In contrast, only a few closed analytic solutions are known for energy-dependent Green functions in three dimensions. Notable examples are the expressions for the field-free environment, the static uniform electric field [9–11], the static uniform magnetic field [12–14] and combined parallel static electric and magnetic fields [15, 16].

2.3. A sum rule for the total current

Exploiting the time-reversal symmetry relation for the propagator $K(\mathbf{r}, t|\mathbf{r}', 0)^\dagger = K(\mathbf{r}, -t|\mathbf{r}', 0)$, the total current $J(E)$ (14) can be rewritten using equation (15) as

$$J(E) = \frac{1}{\hbar^2} \int_{-\infty}^{\infty} dt e^{iEt/\hbar} \int d^3\mathbf{r} \int d^3\mathbf{r}' \sigma(\mathbf{r})^* K(\mathbf{r}, t|\mathbf{r}', 0) \sigma(\mathbf{r}'). \quad (16)$$

Integration with respect to the energy E , together with the initial condition $K(\mathbf{r}, 0|\mathbf{r}', 0) = \delta(\mathbf{r} - \mathbf{r}')$, leads to the following sum rule for the total current:

$$\int_{-\infty}^{\infty} dE J(E) = \frac{2\pi}{\hbar} \int d^3\mathbf{r} \int d^3\mathbf{r}' \sigma(\mathbf{r})^* K(\mathbf{r}, 0|\mathbf{r}', 0) \sigma(\mathbf{r}') = \frac{2\pi}{\hbar} \int d^3\mathbf{r} |\sigma(\mathbf{r})|^2. \quad (17)$$

3. Sources in a uniform force field

To illustrate the formalism developed in the preceding section, we discuss the specific example of a quantum source of Gaussian shape embedded in a uniform force field \mathbf{F} . Experimentally, this situation is approximately realized in near-threshold photodetachment of negative ions in an electric field [17–21], where the limit of pointlike sources applies. Considerably extended sources emerge when ultra-cold rubidium atoms are continuously released from a trapped Bose–Einstein condensate under the influence of gravity (‘atom lasers’, [22, 23]).

3.1. Propagator and the energy Green function

The Hamiltonian H_{cont} for uniformly accelerated motion with $\mathbf{A}(\mathbf{r}) = \mathbf{o}$ is given by

$$H_{\text{field}} = \frac{\mathbf{p}^2}{2m} - \mathbf{r} \cdot \mathbf{F}. \quad (18)$$

For simplicity, we align the field along the z -axis: $\mathbf{F} = F \hat{e}_z$. The propagator assigned to this Hamiltonian is well known and reads [7, 8, 24]

$$K_{\text{field}}(\mathbf{r}, t|\mathbf{r}', 0) = \left(\frac{m}{2\pi i\hbar t} \right)^{3/2} \exp \left\{ \frac{i}{\hbar} \left[\frac{m}{2t} |\mathbf{r} - \mathbf{r}'|^2 + \frac{Ft}{2} (z + z') - \frac{F^2 t^3}{24m} \right] \right\}. \quad (19)$$

The energy-dependent Green function is also available (see [9–11] for a compact derivation) and may be expressed in terms of Airy functions [25]:

$$G_{\text{field}}(\mathbf{r}, \mathbf{r}'; E) = \frac{m}{2\hbar^2 |\mathbf{r} - \mathbf{r}'|} [\text{Ci}(\alpha_+) \text{Ai}'(\alpha_-) - \text{Ci}'(\alpha_+) \text{Ai}(\alpha_-)], \quad (20)$$

where $\alpha_{\pm} = -\beta[2E + F(z + z') \pm F|\mathbf{r} - \mathbf{r}'|]$, $\beta = [m/(4\hbar^2 F^2)]^{1/3}$, and $\text{Ci}(x) = \text{Bi}(x) + i \text{Ai}(x)$. For further reference, we note that this Green function is invariant with respect to simultaneous shifts of the origin and the energy:

$$G_{\text{field}}(\mathbf{r}, \mathbf{r}'; E) = G_{\text{field}}(\mathbf{r} - \mathbf{r}', \mathbf{o}; E + Fz'). \quad (21)$$

For a compact notation it is suitable to introduce a set of scaled parameters

$$\begin{aligned} \xi &= \beta F x & \rho &= \beta F \mathbf{r} \\ \nu &= \beta F y & \epsilon &= -2\beta E \\ \zeta &= \beta F z & \tau &= t/(2\hbar\beta). \end{aligned} \quad (22)$$

This allows us to express the Green function in integral form via (15) and (19):

$$G_{\text{field}}(\rho, \mathbf{o}; \epsilon) = -2i\beta(\beta F)^3 \int_0^{\infty} \frac{d\tau}{(i\pi\tau)^{3/2}} \exp \left(\frac{i}{\tau} \rho^2 + i\tau(\zeta - \epsilon) - \frac{i\tau^3}{12} \right). \quad (23)$$

3.2. Point-like sources

Initially, we discuss a point-like quantum source in a homogeneous force field F . Assuming an isotropic emission pattern, we may idealize the source $\sigma(\mathbf{r})$ in terms of the Dirac δ -distribution

$$\sigma_\delta(\mathbf{r}) = C\delta(\mathbf{r}), \quad (24)$$

where C denotes some complex constant. We note that for this type of source the sum rule stated in equation (17) is not applicable, since the \mathcal{L}^2 norm of $\delta(\mathbf{r})$ is not defined. Instead, the detailed mechanism behind the source in equation (24) merely influences the emission process through the scaling parameter C , the source strength. The wavefunction generated by $\sigma_\delta(\mathbf{r})$ directly follows from equations (11) and (20)

$$\psi(\mathbf{r}) = C G_{\text{field}}(\mathbf{r}, \sigma; E) \quad (25)$$

and yields analytic expressions for the current density (12) in the field direction

$$j_z(\mathbf{r}, E) = |C|^2 \frac{m\beta F}{2\pi\hbar^3 r^3} \{z[\text{Ai}'(\alpha_-)]^2 + \beta[z(2E + Fz) + Fr^2][\text{Ai}(\alpha_-)]^2\}, \quad (26)$$

and for the total current (14)

$$\begin{aligned} J(E) &= -\frac{2|C|^2}{\hbar} \lim_{r \rightarrow 0} \text{Im}\{G_{\text{field}}(\mathbf{r}, \sigma; E)\} \\ &= \frac{2|C|^2 m\beta F}{\hbar^3} \{[\text{Ai}'(-2\beta E)]^2 + 2\beta E[\text{Ai}(-2\beta E)]^2\}. \end{aligned} \quad (27)$$

In a different context, these expressions are also implicitly contained in [10, 15].

3.3. Gaussian source

Now we turn our attention to more realistic spatially extended sources. Specifically, we consider a source term derived from the wavefunction $\psi_0(\mathbf{r})$ in equation (9) of isotropic Gaussian shape

$$\sigma(\mathbf{r}) = \hbar\Omega\psi_0(\mathbf{r}) = \hbar\Omega N_0 \exp(-r^2/(2a^2)). \quad (28)$$

The parameter a describes the width of the source and $N_0 = a^{-3/2}\pi^{-3/4}$ denotes the proper normalization from the condition

$$\int d^3\mathbf{r} |\psi_0(\mathbf{r})|^2 = 1. \quad (29)$$

To obtain the expressions for the currents generated by a Gaussian source, we start with the derivation of the wavefunction from equation (11). Working in the time-dependent propagator representation (see equation (15)), we can carry out the \mathbf{r}' integrations of Gaussian type in

$$\psi(\mathbf{r}) = -i\Omega N_0 \int_0^\infty dt e^{iEt/\hbar} \int d^3\mathbf{r}' K_{\text{field}}(\mathbf{r}, t|\mathbf{r}', 0) e^{-r'^2/(2a^2)}. \quad (30)$$

Upon introducing the scaled width $\alpha = \beta Fa$ and shifted parameters

$$\tilde{\zeta} = \zeta + 2\alpha^4 \quad \tilde{\epsilon} = \epsilon + 4\alpha^4, \quad (31)$$

the problem is reduced to a single complex integration

$$\psi(\mathbf{r}) = -2i\Lambda(\tilde{\epsilon})\beta(\beta F)^3 \int_{-2i\alpha^2}^\infty \frac{du}{(i\pi u)^{3/2}} \exp\left(\frac{i}{u}\tilde{\rho}^2 + iu(\tilde{\zeta} - \tilde{\epsilon}) - \frac{i u^3}{12}\right). \quad (32)$$

Here, $\Lambda(\tilde{\epsilon}) = \hbar\Omega(2\sqrt{\pi}a)^{3/2}e^{2\alpha^2(\tilde{\epsilon}-4\alpha^4/3)}$, and $\tilde{\rho}^2 = \xi^2 + \nu^2 + \tilde{\zeta}^2$. We moved the temporal integration into the complex plane by substituting $u = \tau - 2i\alpha^2$. The representation

chosen in equation (32) emphasizes the close relationship of $\psi(\mathbf{r})$ to the Green function $G_{\text{field}}(\boldsymbol{\rho}, \boldsymbol{\sigma}; \epsilon)$ in the form (23). To evaluate this integral analytically, we split the path of integration into two sections, one along the real u -axis, the other one along the imaginary u -axis: $\psi(\mathbf{r}) = \psi_{\text{near}}(\mathbf{r}) + \psi_{\text{far}}(\mathbf{r})$. The contribution due to

$$\begin{aligned} \psi_{\text{near}}(\mathbf{r}) &= -2i\Lambda(\tilde{\epsilon})\beta(\beta F)^3 \int_{-2i\alpha^2}^0 \frac{du}{(i\pi u)^{3/2}} e^{i\tilde{\rho}^2/u + iu(\tilde{\zeta} - \tilde{\epsilon}) - iu^3/12} \\ &\sim \Lambda(\tilde{\epsilon}) \frac{2\beta(\beta F)^3 \sqrt{2}\alpha}{\pi^{3/2} \tilde{\rho}^2} e^{-\tilde{\rho}^2/(2\alpha^2)} \end{aligned} \quad (33)$$

is a purely real term which drops off very quickly with increasing distance $\tilde{\rho}$ from the source region. The more interesting far-field contribution $\psi_{\text{far}}(\mathbf{r})$ can be exactly evaluated using the integral representation (23):

$$\psi_{\text{far}}(\mathbf{r}) = -2i\Lambda(\tilde{\epsilon})\beta(\beta F)^3 \int_0^\infty \frac{du}{(i\pi u)^{3/2}} e^{i\tilde{\rho}^2/u + iu(\tilde{\zeta} - \tilde{\epsilon}) - iu^3/12} = \Lambda(\tilde{\epsilon}) G_{\text{field}}(\tilde{\boldsymbol{\rho}}, \boldsymbol{\sigma}; \tilde{\epsilon}). \quad (34)$$

With the help of equation (21) we can cast the last equation into the form

$$\psi_{\text{far}}(\mathbf{r}) = \hbar\Omega(2\sqrt{\pi}a)^{3/2} e^{-ma^2 E/\hbar^2 + m^2 F^2 a^6/(3\hbar^4)} G_{\text{field}}\left(\mathbf{r}, -\frac{m\mathbf{F}}{2\hbar^2} a^4; E\right). \quad (35)$$

This expression displays a remarkable feature of the wavefunction $\psi_{\text{far}}(\mathbf{r})$ originating from a Gaussian source: the extended Gaussian source can be replaced by a virtual point source of the same energy at a location shifted by $m\mathbf{F}a^4/(2\hbar^2)$ from the centre of the Gaussian distribution, carrying the energy-dependent weight $\Lambda(\tilde{\epsilon})$. From this relation, the expressions for the currents due to (28) are conveniently found from the analogous expressions for a point source by just performing the indicated shifts. Neglecting $\psi_{\text{near}}(\mathbf{r})$, the far-field current density reads according to equation (26)

$$\begin{aligned} j_z(\boldsymbol{\rho}, \tilde{\epsilon}) &= 16\sqrt{\pi}\hbar\Omega^2\beta^3 F^2 e^{4\alpha^2(\tilde{\epsilon} - 4\alpha^4/3)} \\ &\times \frac{\alpha^3}{\tilde{\rho}^3} \{ \tilde{\zeta} [\text{Ai}'(\tilde{\epsilon} - \tilde{\zeta} + \tilde{\rho})]^2 + \beta [\tilde{\zeta}(\tilde{\zeta} - \tilde{\epsilon}) + \tilde{\rho}^2] [\text{Ai}(\tilde{\epsilon} - \tilde{\zeta} + \tilde{\rho})]^2 \}. \end{aligned} \quad (36)$$

The same procedure yields the total current. However, since both $\psi_{\text{near}}(\mathbf{r})$ and $\sigma(\mathbf{r})$ are purely real and only the imaginary part of $\psi(\mathbf{r})$ is needed for the evaluation of the total current (see equation (13)), the following expression obtained by shifting the energy in equation (27) is even an exact result:

$$J(\tilde{\epsilon}) = 64\pi^{3/2}\hbar\Omega^2\alpha^3\beta e^{4\alpha^2(\tilde{\epsilon} - 4\alpha^4/3)} \{ [\text{Ai}'(\tilde{\epsilon})]^2 - \tilde{\epsilon} [\text{Ai}(\tilde{\epsilon})]^2 \}. \quad (37)$$

In the limit of extended Gaussian sources, a simple approximation to this formula is available that leads to a geometrical interpretation. We start out with a time-dependent integral formulation of the total current that follows from equations (14) and (23) after the spatial integrations are performed:

$$J(\tilde{\epsilon}) = 32\hbar\Omega^2\alpha^3\beta e^{4\alpha^2(\tilde{\epsilon} - 4\alpha^4/3)} \text{Im} \left\{ \int_0^\infty \frac{i du}{(iu)^{3/2}} e^{-iu\tilde{\epsilon} - iu^3/12} \right\}. \quad (38)$$

The integral is evaluated in the saddle point approximation. Assuming $\alpha \gg \epsilon$, we keep only the leading-order terms of a Taylor expansion in the exponent and prefactor. The resulting current has Gaussian shape:

$$J_{\text{sp}}(\epsilon) = \frac{2\sqrt{\pi}\hbar\Omega^2\beta}{\alpha} e^{-\epsilon^2/(4\alpha^2)}. \quad (39)$$

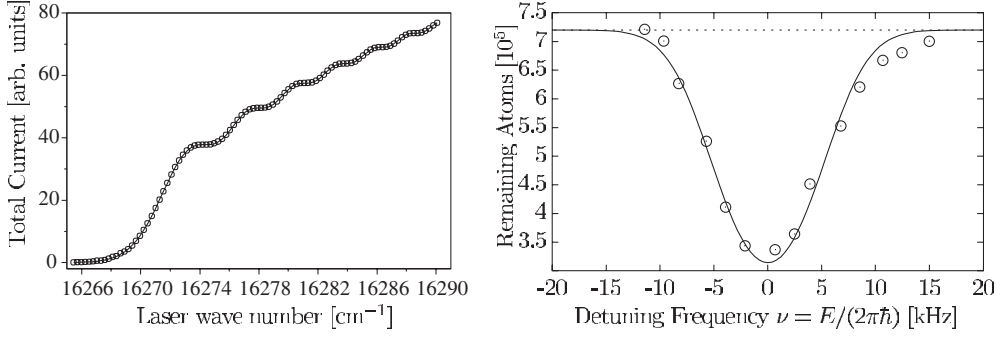


Figure 1. Characteristics of matter waves from sources in uniform force fields. Left-hand panel: total current $J(E)$ in near-threshold photodetachment of S^- in a homogeneous electric field $F = 2.205 \times 10^4 \text{ eV m}^{-1}$. \circ , experimental data of Gibson *et al* [21]. —, theoretical result from (27) with adjusted source strength C . Right-hand panel: number of atoms remaining in a Bose–Einstein condensate $N(T)$ after continuous release of atoms for $T = 20 \text{ ms}$ as a function of the detuning frequency ν . \circ , measurement by Bloch *et al* reported in [26]. —, theoretical prediction according to (37) and (41) with effective Gaussian condensate width $a = 2.8 \text{ }\mu\text{m}$ and outcoupling strength $\Omega = 2\pi \times 105.585 \text{ Hz}$.

This expression is equivalent to the implicit representation

$$J_{\text{sp}}(E) = \frac{2\pi}{\hbar} \int d^3\mathbf{r} |\sigma(\mathbf{r})|^2 \delta(E + Fz). \quad (40)$$

Evidently, the approximation (40) obeys the sum rule (17) for the total current $J(E)$. For extended sources, the energy dependence of $J_{\text{sp}}(E)$ reflects the source structure: by the resonance condition $E + Fz = 0$, the total current probes the density $|\psi_0(\mathbf{r})|^2$ on different slices across the source.

4. Examples: photodetachment and atom laser

As an application for the developed formalism, we would like to discuss two physical systems that have recently undergone experimental evaluation.

4.1. Photodetachment

In photodetachment experiments, negatively charged ions are illuminated by a laser beam to release the surplus electron. If the photon energy closely matches the electron affinity of the ionic species, the detached electron starts out with a well defined minuscule amount of kinetic energy E . Then, the size of the emitting ion is small compared with the initial electronic wavelength $\lambda = h/\sqrt{2mE}$, and details of the atomic structure cannot be resolved: the detached electron wave is solely characterized by its orbital angular momentum (which is in turn fixed by the selection rules of the underlying dipole transition), and allows for a description in terms of a point source $\sigma(\mathbf{r})$. For isotropic (s-wave) emission, the Dirac δ -distribution $\sigma_\delta(\mathbf{r})$ (24) is a viable choice.

In a field-free environment, the electron is emitted simply into a spherical wave, $\psi(\mathbf{r}) \propto e^{ikr}/r$. In this case, the quantum source model presented in section 2 recovers the well established behaviour of the photodetachment cross section near threshold known as Wigner’s law [27], which states that $J(E) \propto \sqrt{E}$. Recently, the question of how the threshold behaviour of the photocurrent is altered in the presence of external fields in the interaction region has

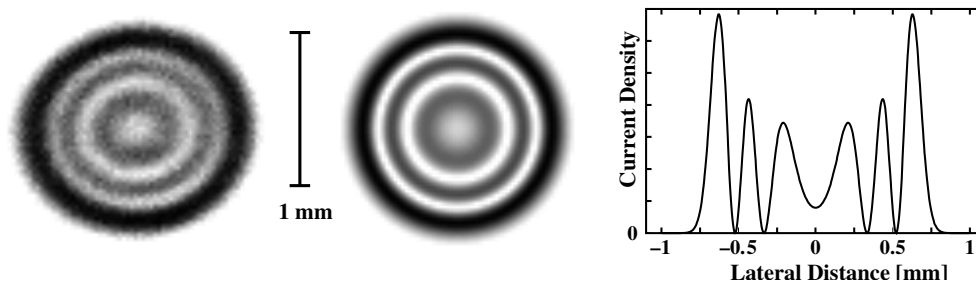


Figure 2. Interference fringes in uniformly accelerated motion. Distribution of electrons in near-threshold photodetachment of O^- in a homogeneous electric field $F = 423 \text{ eV m}^{-1}$. Distance from the source $z = 0.514 \text{ m}$, electron energy $E = 100.5 \text{ } \mu\text{eV}$. Left-hand panel: image recorded by Blondel *et al* [20]. Centre panel: calculation from (26). Right-hand panel: corresponding current density profile as a function of the lateral distance.

found considerable attention [17, 28], and precision experiments were conducted to measure both the energy dependence of the cross section [18, 21] and the corresponding photoelectron distribution [19, 20] for photodetachment in a homogeneous electric field environment. Here, the electric force $\mathbf{F} = -e\mathbf{E}$ accelerating the detached electrons allows for direct comparison with the results presented in section 3.2. The left-hand panel in figure 1 displays the photocurrent measured by Gibson *et al* [21] together with the source-theoretical prediction (27) first obtained in a different fashion by Fabrikant [15]. The agreement is striking. Besides a slow onset below threshold indicating tunnelling emission, the plot prominently features a ‘staircase’ appearance of $J(E)$ modifying Wigner’s law. Although an explanation of this electric-field-induced effect in terms of the closed free-falling orbit has been offered [29], it is more accurately described as the remaining imprint of a remarkable interference pattern in the current density distribution $j_z(\mathbf{r}, E)$ (26).

In a recent series of experiments [19, 20], Blondel *et al* recorded the spatial distribution of the photocurrent on a distant detector plane perpendicular to the applied electric field. One of the impressive images obtained using the ‘photodetachment microscope’ is depicted in figure 2 (left-hand panel), revealing an interference ring pattern of macroscopic size. In the source formalism, the electronic distribution should reflect the local current density $j_z(\mathbf{r}, E)$ pertaining to the Green function $G_{\text{field}}(\mathbf{r}, \mathbf{o}, E)$ (20) in a uniform force field. Indeed, an image calculated from (26) closely resembles the experimental result (centre panel in figure 2). For comparison the corresponding lateral current profile is also shown (right-hand panel).

The conspicuous fringes find a simple semiclassical interpretation in terms of two-path interference: as first pointed out by Demkov [30], within the sector of classically allowed motion two ballistic trajectories will always connect the origin with a given location on the detector. Hence, the uniform electric field effectively acts as a two-slit interferometer [11], providing a sensitive device for the precise determination of electron affinities [20]. Similar results are expected for point sources in parallel electric and magnetic fields where four-path interference takes place [16].

4.2. Atom laser

In section 2 we introduced quantum sources using a coupled two-state model. This model may serve as a simplified description of the atom laser, a coherent beam of particles released from a trapped Bose–Einstein condensate (BEC) [22, 23]. The two states are realized by different

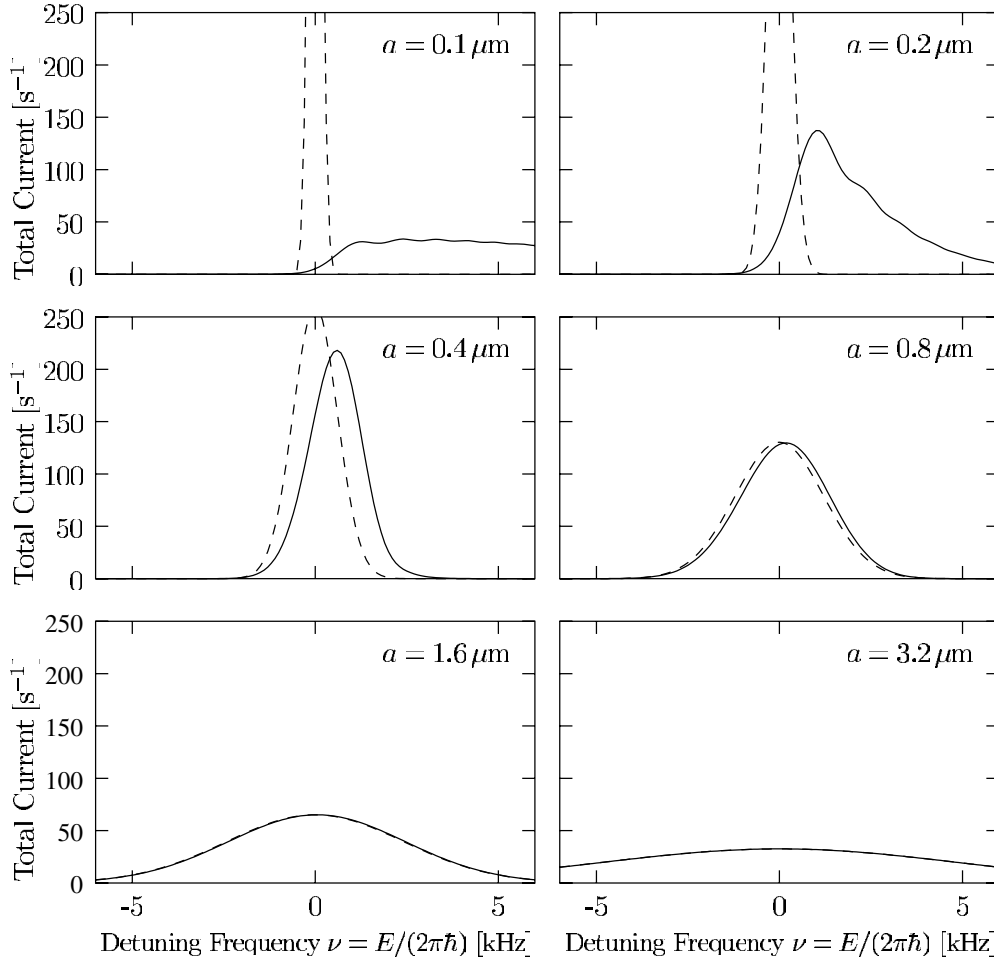


Figure 3. Transition from a point-like source to an extended source. Depicted is the total current $J(E)$ from a Gaussian source of freely falling Rb atoms for different source widths a versus the detuning frequency ν . —, exact currents from (37). - - -, slicing approximation according to (40). The coupling strength is $\Omega = 2\pi \times 100$ Hz. Beam profiles are shown in figure 4.

hyperfine Zeeman levels of Rb. The state $\psi_{\text{trap}}(\mathbf{r})$ is trapped by a magnetic field, whereas the continuum state $\psi_{\text{cont}}(\mathbf{r})$ is not influenced by the trap but subject to gravitational attraction. These states are coupled through an oscillating magnetic field of adjustable frequency with a specific coupling strength $\hbar\Omega$. Near its minimum, the potential for the trapped state is approximately harmonic. For non-interacting particles, the ground state of the condensate in this potential is given by an oscillator wavefunction. In our discussion, we maintain the Gaussian shape of the condensate wavefunction $\psi_0(\mathbf{r})$, but increase its width a in order to account for the repulsive atomic interaction.

The ensuing quantum source $\sigma(\mathbf{r})$ continuously releases Rb atoms (mass m) with an initial energy $E = 2\pi\hbar\nu$ determined by the frequency of the perturbation. These particles are subsequently accelerated by the gravitational force $F = mg$ ($g \approx 9.81 \text{ m s}^{-2}$). From section 3.3 it is possible to predict the efficiency of this process (the total particle current) as well as the spatial distribution of atoms (their current density profile). Experimental data

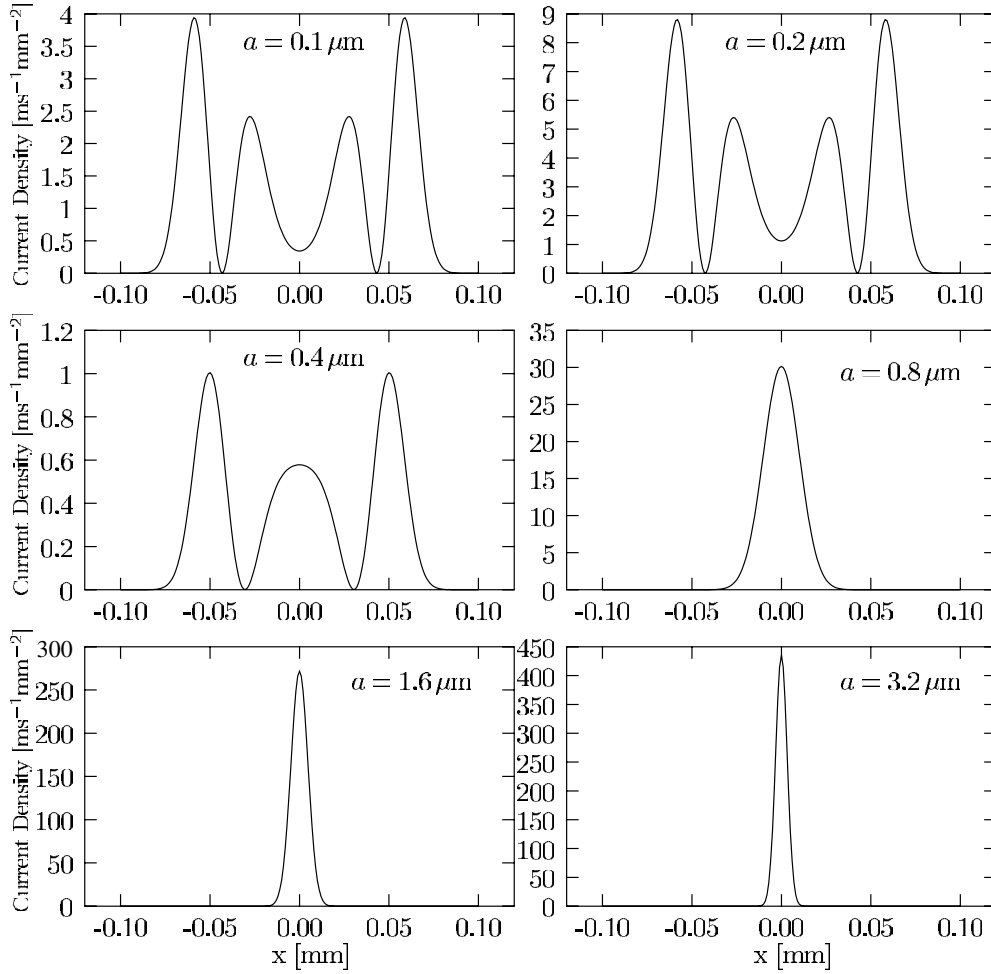


Figure 4. Size dependence of the particle distribution. Profiles of the current density $j_z(x, 0, z, E = 2\pi\nu\hbar)$ for Gaussian sources emitting free-falling Rb atoms. All results are given for $\nu = 2.5$ kHz and $\Omega = 2\pi \times 100$ Hz. There is rotational symmetry about the z -axis (see figure 2). The profiles are calculated from (36) at a distance $z = 1$ mm from the source. The source width is denoted by a (see also figure 3).

concerning the number of remaining condensate atoms $N(T)$ after $T = 20$ ms of atom laser operation are available [26]. Obviously, this number is related to the current by

$$N(T) = N(0) \exp[-J(E)T], \quad (41)$$

where $N(0)$ denotes the initial number of atoms in the BEC and $J(E)$ the total current. Besides the gravitational force, the relevant parameters entering the theoretical prediction for $J(E)$ in equation (37) are the coupling strength $\hbar\Omega$ and the Gaussian width a . In figure 1 (right-hand panel), the calculated number of remaining atoms (41) is compared with the experimental measurement by Bloch *et al* reported in [26]. The coupling frequency Ω used for the calculation is fixed by the sum rule (17) applied to the experimental data, and the effective width $a = 2.8 \mu\text{m}$ (that is actually largely governed by atomic repulsion in the BEC) is obtained from a fit. In contrast to the case of photodetachment, the current characteristics faithfully reproduce the Gaussian shape of the source, as stated by the approximation obtained

by slicing the condensate at height $z = E/F$ (40). However, according to the exact expression for $J(E)$ (37), source theory predicts a dramatic change in behaviour of the total current for smaller condensate sizes as illustrated in figure 3. The plots show both the analytic solution $J(E)$ and the corresponding approximation $J_{\text{sp}}(E)$ for various source widths a . According to the sum rule (17), the area under all curves is the same. For $a > 1 \mu\text{m}$, the two models yield almost identical curves. However, for smaller condensates the differences become noticeable, and for $a < 0.4 \mu\text{m}$ the slicing model fails completely: $J(E)$ becomes asymmetric with respect to $\nu = 0$, and oscillations in the current are prominent. These features are familiar from the photocurrent discussed in the previous section, where we related them to two-path interference in a uniform field (figure 2).

To examine whether similar interference fringes also occur in an ideal atom laser beam, we compute the current density profiles for the set of Gaussian sources displayed in figure 3 from (36). The results from this calculation are shown in figure 4, where we choose as initial energy $E = 2\pi\hbar\nu$ with $\nu = 2.5 \text{ kHz}$. The distance from the source is fixed at $z = 1 \text{ mm}$. In this figure, a distinct ring pattern in the current density prevails for $a \leq 0.4 \mu\text{m}$. The number of fringes diminishes with increasing source width, until for $a \geq 0.8 \mu\text{m}$ the current profile attains an increasingly narrow Gaussian shape. To interpret this behaviour, we first note that for an extended source region the simple concept of two interfering paths originating from a single point in space is not readily applicable. Recalling the particular property of a Gaussian source to act as a virtual point source shifted in space (35), we may recover the concept of interfering paths. However, the effective initial kinetic energy decreases with growing source size (31) and becomes negative for $E < mF^2a^4/(2\hbar^2)$, leading to a ‘virtual’ tunnelling source that emits a beam of Gaussian profile. Its properties are discussed in detail in [11].

5. Conclusion and outlook

Quantum sources that are inserted into the Schrödinger equation provide a convenient and practical tool to assess and solve scattering problems in external potentials. Specifically, we studied point-like and Gaussian quantum sources embedded within a three-dimensional homogeneous force field, and analytical solutions for the resulting particle distribution and total current were obtained. For point sources, the model is in excellent agreement with data gained from near-threshold photodetachment experiments conducted in the presence of an electric field. Available measurements on continuous atom laser beams are in reasonable accordance with the theory presented for an extended source. Dependent on the condensate size, we predict the appearance of a ring pattern related to two-path interference in the atom laser beam released from a single ideal Bose–Einstein condensate.

A modification of the presented theory to comprise sources with definite angular momentum is feasible and will be the subject of a forthcoming publication. Physical applications of this extension include photodetachment experiments involving p-wave emission and the effects of vortices in an ideal Bose–Einstein condensate on the outcoupled atom laser beam.

Acknowledgments

Experimental data on near-threshold photodetachment experiments was kindly provided by C Blondel, N D Gibson and C W Walter. We appreciate useful discussions with these authors as well as P Kramer, W Becker, T Esslinger and T Hänsch. We also thank Kilian Bracher for his patience during the preparation of this paper. Partial financial support by the Deutsche Forschungsgemeinschaft is gratefully acknowledged.

References

- [1] Rodberg L S and Thaler R M 1967 *Introduction to the Quantum Theory of Scattering* (New York: Academic) p 123
- [2] Muller H G 1990 *Comments At. Mol. Phys.* **24** 355
- [3] Becker W, Lohr A and Kleber M 1994 *J. Phys. B: At. Mol. Opt. Phys.* **27** L325
- [4] Lohr A, Becker W and Kleber M 1997 *Multiphoton Processes 1996 (Inst. Phys. Conf. Ser. 154)* (Bristol: Institute of Physics Publishing)
- [5] Economou E N 1983 *Green Functions in Quantum Physics* (Berlin: Springer)
- [6] Bracher C, Riza M and Kleber M 1997 *Phys. Rev. B* **56** 7704
- [7] Kleber M 1994 *Phys. Rep.* **236** 331
- [8] Grosche C and Steiner F 1998 *Handbook of Feynman Path Integrals* (Berlin: Springer)
- [9] Dalidchik F I and Slonim V Z 1976 *Zh. Eksp. Teor. Fiz.* **70** 47 (Engl. transl. 1976 *Sov. Phys.-JETP* **43** 25)
- [10] Li Y L, Liu C H and Franke S J 1990 *J. Acoust. Soc. Am.* **87** 2285
- [11] Bracher C *et al* 1998 *Am. J. Phys.* **66** 38
- [12] Bakhrakh V L and Vetchinkin S I 1971 *Teor. Mat. Fiz.* **6** 392 (Engl. transl. 1971 *Theor. Math. Phys.* **6** 283)
- [13] Gountaroulis G 1972 *Phys. Lett. A* **40** 132
- [14] Dodonov V V, Malkin I A and Man'ko V I 1975 *Phys. Lett. A* **51** 133
- [15] Fabrikant I I 1991 *Phys. Rev. A* **40** 258
- [16] Kramer T, Bracher C and Kleber M 2001 *Europhys. Lett.* **56** 471
- [17] Bryant H C *et al* 1987 *Phys. Rev. Lett.* **58** 2412
- [18] Baruch M C *et al* 1991 *Phys. Rev. A* **45** 2825
- [19] Blondel C, Delsart C and Dulieu F 1996 *Phys. Rev. Lett.* **77** 3755
- [20] Blondel C *et al* 1999 *Eur. Phys. J. D* **5** 207
- [21] Gibson N D *et al* 2001 *Phys. Rev. A* **64** 061403(R)
- [22] Mewes M-O *et al* 1997 *Phys. Rev. Lett.* **78** 582
- [23] Bloch I, Hänsch T W and Esslinger T 1999 *Phys. Rev. Lett.* **82** 3008
- [24] Kennard E H 1927 *Z. Phys.* **44** 326
- [25] Abramowitz M and Stegun I A 1965 *Handbook of Mathematical Functions* (New York: Dover)
- [26] Gerbier F, Bouyer P and Aspect A 2001 *Phys. Rev. Lett.* **86** 4729
- [27] Wigner E P 1948 *Phys. Rev.* **73** 1002
- [28] Blumberg W A M, Jopson R M and Larson D J 1978 *Phys. Rev. Lett.* **40** 1320
- [29] Du M L and Delos J B 1989 *Phys. Lett. A* **134** 476
- [30] Demkov Yu N, Kondratovich V D and Ostrovskii V N 1981 *Pis. Zh. Eksp. Teor. Fiz.* **34** 425 (Engl. transl. 1982 *JETP Lett.* **34** 402)